Scattering analysis of arbitrarily shaped cylinders in a focused beam system

R. Shavit
T. Wells
A. Cohen

Indexing terms: Antennas, Scattering

Abstract: The scattering from an arbitrarily shaped cylinder is characterised by its induced field ratio (IFR) and its scattering pattern. The paper describes how a focused beam system is used to determine the scattering characteristics of an arbitrarily shaped cylinder. The fields of the transmitting and receiving antennas are described by equivalent fundamental Gaussian beams. An analytical procedure based on the computation of the coupling between the Gaussian beams in the focused beam system and the scattered field is used to determine the IFR and the scattering pattern of the cylinder. The results obtained by this method verify well with the scattering characteristics computed analytically or numerically by the method of moments or finite element method.

1 Introduction

Large sandwich and metal space frame radomes are assembled from many panels connected together with seams or metal beams. These seams/beams introduce scattering effects that degrade the overall electromagnetic performance (transmission loss and radiation pattern perturbation) of the antenna enclosed in the radome. This effect can be evaluated by considering the superposition (array factor) of all scattered fields from all the seams/beams in front of the antenna. The cornerstone for such a computation is the knowledge of the scattering characteristics from an individual seam/beam, which can be approximated from the scattering characteristics of an infinite extent cylinder with the same cross-section as the seam/beam in the radome. Therefore, the ability to compute and measure the scattering characteristics of an arbitrarily shaped cylinder is essential to the entire scattering analysis. The scattering characteristics of an arbitrarily shaped cylinder are characterised by its forward scattering value (IFR) and its scattering pattern. This concept was introduced by Kay [1] for modelling metal space frame radomes. The IFR is defined as the ratio of the forward scattered field to the hypothetical field radiated in the forward direction by the plane wave in the reference aperture of width equal to the shadow of the geometrical cross-section of the cylinder on the incident wavefront [2]. Low IFR is an indication of low scattering effect in the forward direction. Some deficiencies in the IFR approach [1] to predict the total scattered field from all the beams/seams in a radome have been discussed in [3] and a more rigorous approach based on the full 2×2 scattering matrix from an individual beam/seam for general incident field conditions combined with the plane wave spectrum approach was applied to metal space frame radomes [4] and dielectric space frame radomes [5].

Analytical computations of the scattering characteristics from cylinders can be performed for canonical cross-sections like those of the circle and ellipse, but for arbitrarily shaped cylinders numerical computations with techniques like MoM (method of moments) [6] and FEM (finite element method) [7] are required. These numerical techniques are in many cases quite laborious and time-consuming. Consequently, in many practical instances, to speed up the developing process, control manufacturing processes and verify the numerical computation an accurate measurement technique of the IFR and the scattering pattern is required. Rusch [2] developed the IFR concept and suggested an experimental procedure to measure its value in the far field for an arbitrarily shaped cylinder. This procedure lacks the capability to measure its scattering pattern. Shavit [8] proposed an alternative technique to determine both the IFR and the scattering pattern of an arbitrarily shaped cylinder based on near-field probing. However, both methods lack the ability to filter out the reflections from surrounding objects, which may compromise the accuracy of the measurement.

The current paper describes a new combined experimental and numerical procedure to determine the scattering characteristics, IFR and scattering pattern of arbitrarily shaped cylinders using a focused beam system. The unique feature of the focused beam system, which produces a highly collimated beam between the transmitting and receiving ends, helps to reduce measurement errors due to specular and diffuse reflections from adjacent objects in comparison to the errors present in a previous measurement system [2], where wide beamwidth antennas are used on the transmitting and receiving ends.

IEE Proceedings online no. 19982042

Paper first received 25th November 1997 and in revised form 25th February 1998

R. Shavit is with the Department of Electrical and Computer Engineering, Ben Gurion University, PO Box 654, Beer-Shera 84105, Israel

T. Wells and A. Cohen are with Electronic Space Systems Corporation, Concord, MA 01742-4697, USA

2 Method description

The schematic configuration of the measurement system is shown in Fig. 1. The system is comprised of two circular identical dielectric lenses L_1 and L_2 with diameter D and two feed horns H_1 and H_2 with aperture dimensions $A \times B$ and linear polarisation. Each lens is designed to have two focal points located at distances f_1 and f_2 from the opposite sides of the lens surface. The actual distance of the feed horn phase centre from the lens surface is d_1. In principle it is desired that $f_1 = d_1$; however, due to the movement of the feed horn phase centre with frequency this requirement is not achieved perfectly. The energy radiated by the feed horn H_1 is captured by the L_1 lens, focused on the opposite side to the common focal point of the two lenses at a distance d_2 from the lens surface, radiated into the lens L_2 and focused again into the receiving feed horn H_2. We define the focal plane of the system as the plane passing through the internal (common) focal point of the two lenses and perpendicular to the system axis. In the measurement to be described the cylindrical scatterer will be located in this focal plane on the system axis. In such a system most of the energy is transferred from one feed horn to the other feed horn without significant losses and reflection interference from surrounding objects. The contours of the lenses can be computed by geometrical optics as described in [9].

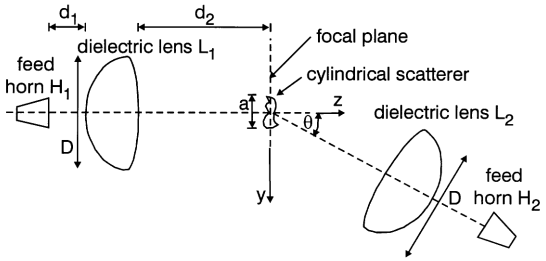

Fig.1 *Schematic configuration of focused beam system*

In this paper we made the assumption that the propagation mechanism of the focused beam system can be described by fundamental Gaussian beams [10]. In addition, we made the assumption that the two lenses act as phase transformers [11], each providing a phase advancement approximately proportional to the square of the distance r of a ray from the axis of propagation, $\Delta\phi = \pi r^2/\lambda f$, in which $1/f = 1/f_1 + 1/f_2$. This phase advancement transforms the diverging Gaussian beam of feed horn H_1 (cf. Fig. 1) to a converging Gaussian beam with minimum waists w_{0x} and w_{0y}, representing the field distribution in the x and y directions, respectively. Since the waists w_{0x} and w_{0y} are close in value, we can define an equivalent quasi-circular minimum waist in the focal plane by $w_{0l} = \sqrt{w_{0x}w_{0y}}$. The minimum waist of the internal Gaussian beam, w_{0l}, is located a distance d_2 from the lens surfaces on both sides. By symmetry, the converging Gaussian beam is transformed into an outward Gaussian beam (at the focal plane $z = 0$) captured by the second lens and transformed into an inward Gaussian beam captured by feed horn H_2 as shown in Fig. 1. In the internal focal plane, we obtain a minimum Gaussian beam waist w_{0l} with constant phase distribution. The received signal is set to zero (amplitude and phase) before the cylinder is moved into the focal plane. Then, the cylinder is brought into the focal plane on the system axis, and the relative amplitude $\Delta\alpha$ and phase $\Delta\phi$ of the received signal $R(y) = \Delta\alpha e^{j\Delta\phi}$ is recorded. Then the receiving lens is rotated in predetermined angular increments on an arch with its centre of rotation located on the system axis in the focal plane. For each angular point two readings are taken with and without the cylinder.

2.1 System analysis without the scatterer

The angular dependence of the transmission loss between the two feed horns is proportional to the coupling between the inward and outward Gaussian beams in the focal plane, $C_c(\theta)$. The electric field distribution in the focal plane ($z = 0$) of the inward Gaussian beam, $f_t(x, y)$, can be described by [10]

$$f_t(x,y) = f_{0t}\exp\left(-\frac{x^2}{w_{0x}^2} - \frac{y^2}{w_{0y}^2}\right) \tag{1}$$

while the electric field distribution of the outward Gaussian beam, $f_r(x, y)$, in the focal plane can be expressed in a similar fashion, but with the addition of a linear progressive phase due to the nonalignment of this beam with the system axis (cf. Fig. 1),

$$f_r(x,y) = f_{0r}\exp\left(-\frac{x^2}{w_{0x}^2} - \frac{y^2}{w_{0y}^2}\right)\exp(-jk\sin\theta y) \tag{2}$$

f_{0t} and f_{0r} are normalisation factors. The coupling factor $C_c(\theta)$ between the two Gaussian beams is computed by performing a two-dimensional integral in the focal plane over the product of the two electric field distributions f_r and f_t [10],

$$C_c(\theta) = \int_{-\infty}^{\infty}\int_{-\infty}^{\infty} f_t f_r^* dxdy \tag{3}$$

Substitution of eqns. 1 and 2 into eqn. 3, and evaluation of the integral, results in

$$C_c(\theta) = C_0\exp\left[-\frac{1}{2}\left(\frac{w_{0y}\pi}{\lambda}\sin\theta\right)^2\right] \tag{4}$$

in which $C_0 = f_{0r}f_{0t}w_{0x}w_{0y}\pi/2$ is the coupling coefficient between the two beams, when the two lenses are aligned ($\theta = 0$). The coupling factor $C_c(\theta)$ can be either computed through eqn. 4 or measured directly.

2.2 System analysis with the scatterer

In this case the signal received by feed horn H_2 is proportional to the coupling, $C_t(\theta)$ of the outward Gaussian beam with the total electric field in the vicinity of the cylinder in the focal plane. The total electric field is the superposition of the electric field without the cylinder and the electric field scattered by the cylinder. Thus

$$C_t(\theta) = \int_{-\infty}^{\infty}\int_{-\infty}^{\infty}(f_t + f_{sp})f_r^* dxdy \tag{5}$$

in which $f_{sp}(x, y)$ is the scattered electric field in the focal plane ($z = 0$). $f_{sp}(x, y)$ can be approximated by

$$f_{sp}(x,y) = \begin{cases} f_s(y)\exp\left(-\frac{x^2}{w_{0x}^2} - \frac{y^2}{w_{0y}^2}\right); & |y| \le \frac{a}{2},\ |x| < \infty \\ 0 & \text{elsewhere} \end{cases} \tag{6}$$

where $f_s(y)$ is the scattered field distribution from the cylinder in the focal plane for uniform plane wave illumination and a is the projected width of the cylinder

on the focal plane. In a similar fashion to the computation of the coupling in the focal plane without the cylinder, we can compute the coupling $C_s(\theta)$ between the scattered field by the cylinder and the nonaligned outward Gaussian beam; evaluation of such an integration results in

$$C_s(\theta) = C_{s0} \int_{-a/2}^{a/2} f_s(y) \exp\left(-2y^2/w_{0y}^2\right) \exp(jk \sin\theta y)\, dy \tag{7}$$

in which $C_{s0} = f_{0r} w_{0x} \sqrt{\pi}/2$. At this point we can make an interesting observation that $C_s(\theta)$ has the form of the far field radiation pattern [12] of the field distribution $f_s(y)$ exp(-$2y^2/w_{0y}^2$) excited in the focal plane. One should remember that we are interested in the radiation pattern from the field distribution $f_s(y)$ (uniform plane illumination).

In the actual measurement, we normalise the received signal at each angle to C_0 the value recorded at $\theta = 0$ without any scatterer. Substitution of eqns. 7 and 4 into eqn. 5 yields

$$\frac{C_t(\theta) - C_c(\theta)}{C_0} = \frac{\sqrt{2/\pi}}{f_{0t} w_{0y}} \int_{-a/2}^{a/2} f_s(y) \exp(-2y^2/w_{0y}^2) \exp(jk \sin\theta y) dy \tag{8}$$

2.3 Scattering pattern evaluation

The scattering radiation pattern $E_s(\theta)$ for uniform plane wave illumination can be computed by [12]

$$E_s(\theta) = \int_{-a/2}^{a/2} f_s(y) \exp(jk \sin\theta y) dy \tag{9}$$

On the other hand, in a focused beam system the received signal (eqn. 8) is proportional to a similar quantity, $E_{sp}(\theta)$, defined as

$$E_{sp}(\theta) = \int_{-a/2}^{a/2} f_s(y) \exp(-2y^2/w_{0y}^2) \exp(jk \sin\theta y) dy \tag{10}$$

If we compare $E_{sp}(\theta)$ with the scattering radiation pattern, $E_s(\theta)$, one can recognise that for cylinders with $a/w_{0y} << 1$, $E_{sp}(\theta)$ is a very good estimate of the scattering radiation pattern. In cases that $a/w_{0y} \geq 1$ a different approach should be adopted. Inspection of eqn. 10 reveals that the field distribution $f_s(y)$ can be evaluated by inverse Fourier transform of eqn. 10 such that

$$f_s(y) = \frac{\exp(2y^2/w_{0y}^2)}{2\pi} \int_{-\infty}^{\infty} E_{sp}(u) e^{-juy} du \tag{11}$$

in which $u = k \sin\theta$. In the case that $a/\lambda > 1$, $E_{sp}(u)$ is a bandlimited function and knowledge of its behaviour in the visible range ($-k \sin\theta_{max}$, $k \sin\theta_{max}$), where θ_{max} is the maximum measurement angle, would be sufficient to truncate the integration to only the visible range without significant loss in accuracy. Once $f_s(y)$ is evaluated through eqn. 11, we can compute the scattering radiation pattern through eqn. 9. Moreover, if $E_{sp}(u)$ is a bandlimited function, we can use the Nyquist sampling theorem to reduce the amount of angular measurements without compromising the accuracy of the reconstructed scattering pattern.

2.4 IFR computation

The IFR of an arbitrarily shaped cylinder is given by [2]

$$IFR = -\frac{Z_0}{2aE_0} \oint_{S_1} J_{sx} e^{jk\rho' \sin\phi'} dl \tag{12}$$

in which $Z_0 = 120\,\pi$, J_{sx} is the induced current distribution on the cylinder and E_0 is the intensity of the incident electric field. In the case that most of the scattered energy propagates in the forward half medium, an alternative representation of the *IFR* can be derived in terms of the tangential scattered electric field, $f_s(y)$, in the projected aperture of the cylinder on the focal plane,

$$IFR = \frac{\int_{-a/2}^{a/2} f_s(y) dy}{E_0 a} \tag{13}$$

If we denote the change in amplitude by $\Delta\alpha$(dB) and the change in phase by $\Delta\phi$, when the cylinder is brought to the focal plane on the system axis and we use eqns. 13 and 8 with $E_0 = f_{0t}$, we can express the *IFR* by

$$IFR = \left(10^{\frac{\Delta\alpha}{20}} e^{j\Delta\phi} - 1\right) \sqrt{\frac{\pi}{2}} \frac{w_{0y}}{a} \times \frac{\int_{-a/2}^{a/2} f_s(y) dy}{\int_{-a/2}^{a/2} f_s(y) \exp(-2y^2/w_{0y}^2) dy} \tag{14}$$

As a first order approximation, we can assume that $f_s(y)$ = const in the projected width. In this specific case, we obtain a very simple and compact expression for the *IFR*:

$$IFR = \left(10^{\frac{\Delta\alpha}{20}} e^{j\Delta\phi} - 1\right) \frac{1}{\mathrm{erf}\left(\frac{a}{\sqrt{2} w_{0y}}\right)} \tag{15}$$

in which erf(x) = $2/\sqrt{\pi} \int_0^x e^{-t2}\, dt$ is the error function.

3 Numerical results

A focused beam system was built to validate the theoretical approach outlined previously. Two AEL model H-1498 antenna horns operating in the frequency range 2–18 GHz were chosen as feeds with almost constant 10 dB beamwidth in both *E* and *H* planes over the entire frequency bandwidth. The diameter of the lens was chosen to be 55.9 cm and it was manufactured from material with dielectric constant 2.3. The lens focal distances f_1 and f_2 were chosen as 53.3 cm and 203.2 cm, respectively. Because of the variation of the feed horn phase centre location with frequency we had to determine d_2 for each test frequency. This task was accomplished by probing the amplitude and phase of the electric field in front of lens L_1. The distance d_2 was chosen as the distance for which the maximum phase flatness was obtained. Fig. 2 shows a typical recorded near-field signal (amplitude and phase) at the minimum waist location for 12 GHz as the operating frequency

and vertical polarisation. The abscissa represents the relative distance along the y axis in front of lens L_1. One can observe Gaussian amplitude tapering and the phase flatness of the probed electric field. In this case the distance d_1 from the feed horn to the lens was found to be 49.2cm and the distance d_2 from the probe to the lens was 166.3cm. The Gaussian beam waist sizes, w_{0x} and w_{0y}, in the focal plane were measured to be 6.4cm and 6.8cm, respectively, at –8.7dB points (the field is e^{-1} of its value on axis). Investigation of the frequency bandwidth (flat phase distribution in the focal plane) of the lens system revealed that the operating frequency range is ~ 8–15GHz.

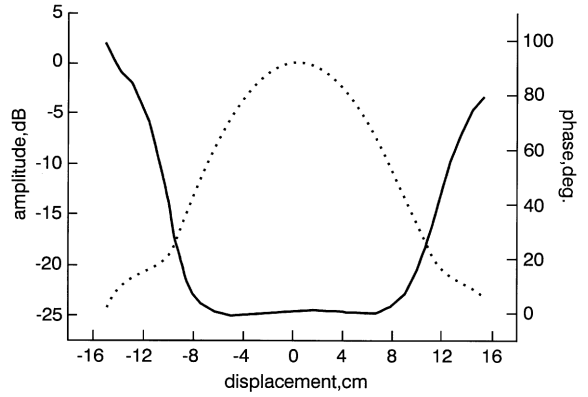

Fig.2 *Recorded near-field signal (amplitude and phase) at minimum waist location in local plane at 12GHz and vertical polarisation*
——— phase
– – – – amplitude

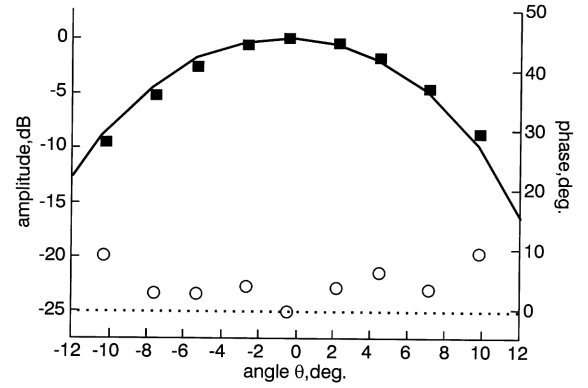

Fig.3 *Recorded signal (amplitude and phase) proportional to the coupling factor $C_c(\theta)$ without the scatterer at 12GHz and vertical polarisation*
■ amplitude (measured)
○ phase (measured)
——— amplitude (computed)
– – – – phase (computed)

Two cylinders – a 1.37 × 5.16cm rectangular metal beam and a 1.2 × 5.71cm plastic beam with ε_r = 5.0 – were tested at 12GHz for both vertical (VP) and horizontal (HP) polarisations and for two incident angles (broadside and narrow side). Fig. 3 shows the comparison between the computed (eqn. 4) and measured angular dependence (amplitude and phase) of the coupling factor $C_c(\theta)$ without the cylindrical scatterer at 12GHz and vertical polarisation. One can observe a good agreement between the two. Fig. 4 shows a typical recorded signal (amplitude and phase) throughout the angular movement of the receiving end (horn H_2 and lens L_2) with the plastic beam located in the focal plane and illuminated by a vertical polarised wave on its broadside. Owing to the physical constraints of the measurement setup, the angular extent of our focused beam was θ_{max} = 70°. The recorded data were plugged into eqn. 8 and processed with an FFT algorithm to evaluate the field distribution of the scatterer, $f_s(y)$, in the focal plane using eqn. 11. The FFT algorithm requires the value of $E_{sp}(u)$ in equal increments du.

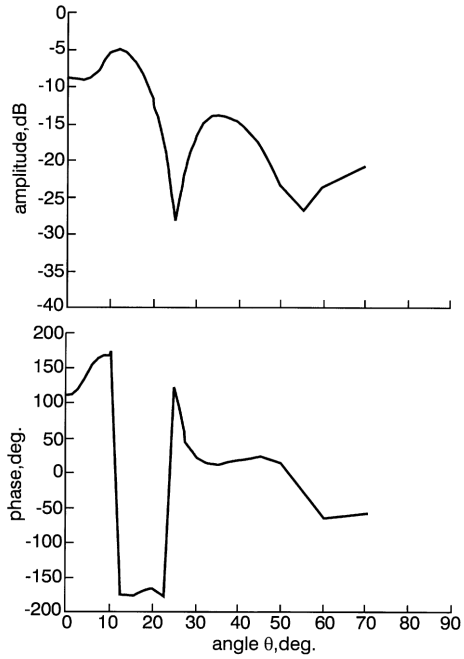

Fig.4 *Recorded signal (amplitude and phase) proportional to the coupling factor $C_t(\theta)$ with dielectric beam 1.2 × 5.71cm in focal plane, illuminated on its broadside at 12GHz and vertical polarisation*
——— measured

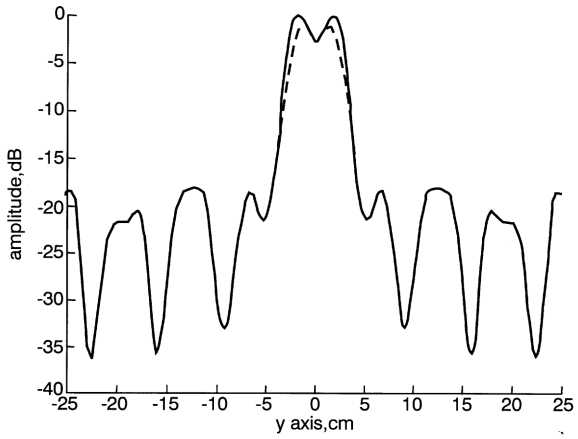

Fig.5 *Electric field distribution in focal plane for uniform plane illumination $f_s(y)$ and for Gaussian beam illumination $f_{sp}(y)$ of a dielectric beam 1.2 × 5.71cm illuminated on its broadside at 12GHz and vertical polarisation*
——— $f_s(y)$
– – – – $f_{sp}(y)$

Therefore, we had to interpolate the function $E_{sp}(\theta)$ to obtain its value at the required u locations. Moreover, if we denote the number of samples for the FFT by N_u, the increment on the u axis will be $du = k \sin\theta_{max}/N_u$ and the corresponding increment on the y axis (Nyquist sampling theorem) will be $dy = \lambda/\sin\theta_{max}$. One can observe that the larger θ_{max} is, the better the resolution of the field distribution on the y axis. Fig. 5 shows the field distribution $f_s(y)$ (uniform field illumination) compared to $f_{sp}(y)$ field distribution (Gaussian field illumination). It is interesting to note the tapering caused by the Gaussian beam illumination in the projected area of the dielectric beam on the focal plane. Fig. 6 shows the comparison among the computed scattering pattern by FEM, the direct measured scattering pattern as a result of $f_{sp}(y)$ distribution, $E_{sp}(\theta)$ and the reconstructed

scattering pattern due to $f_s(y)$ distribution, $E_s(\theta)$. One can observe that a good agreement in the main beam and in the sidelobe level is obtained, when we compare the computed and the reconstructed pattern, while the direct measured scattering pattern $E_{sp}(\theta)$ is characterised by lower sidelobes as a result of the tapering in its field distribution introduced by the Gaussian beam illumination. This tapering effect is insignificant for very narrow cylinders and in these cases $E_{sp}(\theta)$ can be considered as a reliable scattering pattern. The ripple in the reconstructed pattern at $\theta \approx 12°$ and 23° is probably caused by corrupted phase measurement data.

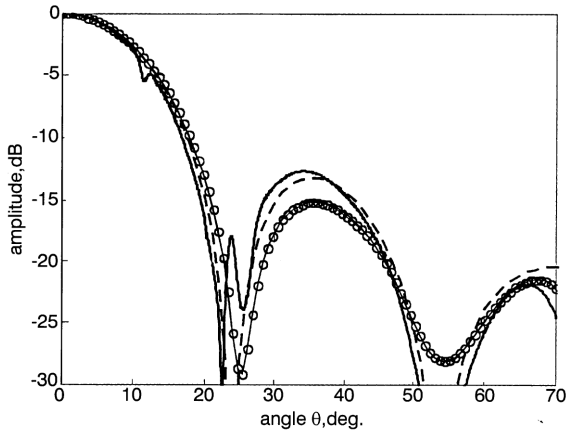

Fig. 6 *Comparison among computed, direct measured and reconstructed scattering patterns of dielectric beam 1.2 × 71 cm illuminated on its broadside at 12 GHz and vertical polarisation*
——— reconstructed
○○○ measured
– – – – computed

The data from all measurements taken for both the plastic and metal beams was processed to obtain the reconstructed field distribution $f_s(y)$, and the corresponding *IFR* was computed based on eqn. 14. The results obtained were compared to the *IFR* values computed through eqn. 15 and to the *IFR* values computed numerically by MoM for the metallic beam and by FEM for the plastic beam. Computation results of the *IFR* for the various types of cylinders by the three methods at 12 GHz are shown in Table 1.

One can observe a good agreement between the numerical computation (MoM and FEM) and the computed values using the reconstructed field distribution $f_s(y)$ (eqn. 14). It is interesting to note that we obtained fairly good agreement with the results obtained with the first order approximation, eqn. 15. This fact indicates that in many cases, if we are interested just in the *IFR* value, it would be sufficient to take only one measurement with the cylinder in the focal plane, without the need to take any angular measurements.

4 Summary

A new combined experimental and numerical procedure to determine the scattering characteristics, *IFR* and scattering pattern of arbitrarily shaped cylinders using a focused beam system have been presented. The analysis is based on the assumption that the electric fields between the lenses can be described by fundamental Gaussian beams. An analytical procedure based on the computation of the coupling between the Gaussian beams in the focused beam system and the scattered field is used to determine the *IFR* and the scattering pattern of the cylinder. A compact and straightforward formulation for the *IFR* computation was derived. The results obtained by this method verify well with the scattering characteristics computed analytically or numerically by the method of moments or finite element method. The unique features of the focused beam system reduce measurement errors caused by specular and diffuse reflections from adjacent objects. The new method complements Rusch's method. The information obtained on the scattering pattern helps to refine the calculations of the scattering analysis for large space frame radomes.

5 Acknowledgments

The authors wish to express their thanks to A. Mantz and C. Slotta for performing the measurements and to T. Monk and J. Sangiolo for very helpful and fruitful discussions. All are associated with ESSCO, Concord, MA, USA.

6 References

1 KAY, A.F.: 'Electrical design of metal space-frame radomes', *IEEE Trans.*, 1965, AP–13, pp. 188–202
2 RUSCH, W.V.T., HANSEN, J.A., KLEIN, C.A., and MITTRA, R.: 'Forward scattering from square cylinders in the resonance region with application to aperture blockage', *IEEE Trans.*, 1976, AP–24, pp. 182–189
3 ROBINSON, A.J., BENNETT, J.C., SMITH, F.C., and CHAMBERS, B.: 'Evaluation of the EM performance of large ground based radomes'. Proceedings of the 6th *Electromagnetic structures* conference, Frierichshafen, Germany, September 1991, pp. 227–235

Table 1: Comparison between measured and computed IFR values

	Vertical polarisation						Horizontal polarisation					
	IFR amplitude			IFR phase, deg.			IFR amplitude			IFR phase, deg.		
Cylinder type	MoM/ FEM	Using reconst. distr. eqn. 14	First order approx. eqn. 15	MoM/ FEM	Using reconst. distr. eqn. 14	First order approx. eqn. 15	MoM/ FEM	Using reconst. distr. eqn. 14	First order approx. eqn. 15	MoM/ FEM	Using reconst. distr. eqn. 14	First order approx. eqn. 15
Plastic a = 1.2 cm	2.24	2.19	2.187	164.3	166.1	165.5	1.05	0.96	0.91	125.9	132.5	129.1
Plastic a = 5.71 cm	1.91	1.93	1.924	158.8	162.4	163.07	1.79	1.84	1.72	162.6	164.0	167.48
Metal a = 1.37 cm	2.42	2.3	2.54	151.8	153.4	152.34	1.2	1.1	1.02	–165.3	–168.3	–144.3
Metal a = 5.16 cm	1.14	1.20	1.1	172.6	171.6	172.6	0.98	1.0	1.06	–176.6	176.1	179.2

4 JOY, E.B., EPPLE, M.B., and PUNNETT, M.B.: 'Analysis of MSF radome using plane wave spectra techniques'. Proceedings of the joint 3rd international conference on *Electromagnetics in aerospace applications* and the 7th European *Electromagnetic structures* conference, Torino, Italy, September 1993, pp. 181–184
5 ROBINSON, A.J., CHAMBERS, B., and BENNETT, J.C.: 'Technique for predicting the electromagnetic performance of impedance-loaded dielectric space-frame radome components', *IEE Proc. Radar, Sonar Navig.*, 1997, 144, (1), pp. 1–8
6 RICHMOND, J.H.: 'Scattering by a dielectric cylinder of arbitrary cross-section shape', *IEEE Trans.*, 1965, AP–13, pp. 334–341
7 JIN, J.: 'The finite element method in electromagnetics' (Wiley, New York, 1993)
8 SHAVIT, R., COHEN, A., and NGAI, E.C.: 'Characterization of the scattering parameters from arbitrary shaped cylinders by near-field probing', *IEEE Trans.*, 1995, AP–43, pp. 1–5
9 LO, Y.T. and LEE, S.W.: 'Antenna handbook: theory applications, and design' (Van Nostrand Reinhold, New York, 1988)
10 GOLDSMITH, P.F.: 'Infrared and millimeter waves' (Academic Press, New York, 1982)
11 GOODMAN, J.W.: 'Introduction to Fourier optics' (McGraw-Hill, New York, 1968)
12 ELLIOTT, R.S.: 'Antenna theory and design' (Prentice-Hall, New Jersey, 1981)